Bulg. J. Phys. **43** (2016) 279–295

Excitonic and Vibronic Spectra in the Model of a 3D Hexagonal Donor–Acceptor Crystal*

I. J. Lalov, **I. Zhelyazkov**
Faculty of Physics, St. Kliment Ohridski University of Sofia,
5 James Bourchier Blvd., 1164 Sofia, Bulgaria

Received *2 December 2016*

Abstract. This paper explores the excitonic spectra and their manifestation in the linear absorption in the 3D model of a hexagonal donor–acceptor crystal of the crystallographic point group $\bar{6}$. A similar two-component crystal of alternative parallel layers with hexagonal order in each layer has been synthesized. Two types of excitons, Frenkel excitons (FEs) and charge-transfer excitons (CTEs) have been considered along with their coupling and the exciton–phonon coupling with one mode of intramolecular vibrations. We find also the symmetry allowed combinations of FEs and CTEs. The excitonic and vibronic spectra have been calculated and numerically simulated.

PACS codes: 71.35.Cc, 73.20.Mf, 78.20.Bh

1 Introduction

This paper has been inspired, at least partly, by the synthesis of a two-component hexagonal crystal of organic compounds [1]. As a result of the crystal engineering the authors obtained and investigated the structure of a molecular complex crystal of alternating and perfectly flat layers of trimethylisocyanurate and of 1,3,5-trinitrobenzene, respectively. In each layer the molecules create a hexagonal two-dimensional sublattice and the neighbor interlayer interactions are characterized as "weak and viable." This type of structure of the real 3D crystal effectively reduces the dimensionality to two 2D flat lattices.

In our theoretical treatment of the excitonic and vibronic spectra we study the model of that layered hexagonal crystal with two alternating 2D hexagonal lattices each of one compound only. We suppose the manifestation of two types of excitons: (a) Frenkel excitons (FEs) which stem from electronic excited state of the molecule of one sublattice, and (b) charge-transfer excitons (CTEs) corresponding to a pair of ionized molecules (positive and negative ions) of the two

*This article is based on a talk given at the 3rd National Congress on Physical Sciences, 29 Sep. – 2 Oct. 2016, Sofia.

different compounds treated as donor (D) and acceptor (A), respectively. The intramolecular mode which creates the vibronic spectra can be both vibration of the donor or acceptor molecule. In our study, we apply the results of the analysis of the excitonic spectra of 1D donor–acceptor lattice [2] and also of 2D ones [3]. Our model certainly does not describe in detail the optical properties of the aforementioned crystal, but it can be a good approach to their treatment in layered molecular structures of high symmetry.

The fundament of our study is the general theory of excitons in molecular structures [4, 5] along with the concept and studies of CTEs [5–7]. In the same time, we make a classification of FEs and CTEs states using the symmetry of excitations in the crystallographic point group $\bar{6}$ (C_{3h}) – see, e.g., [8]. It is interesting to obtain the combinations of CTEs which correspond to all representations of that group of symmetry. Through the calculations of the linear optical susceptibilities based on the vibronic approach [9], we simulate the linear absorption spectra in which the contributions of the transition dipole moments FEs and CTEs are the most important. But owing to the impact of the transition moments of higher multipoles some mute exciton states could manifest themselves weakly in the linear absorption spectra, too.

The paper's outline is as follows: in Sec. 2 we describe the structure of the model crystal and make the symmetry analysis of CTEs states in the crystallographic point group $\bar{6}$. Section 3 contains analogous analysis of FEs states and we obtain the Hamiltonian which includes the FEs–CTEs coupling part. Section 4 describes the exciton–phonon coupling, while Secs. 5 and 6 deal with the calculations of the linear optical susceptibilities in the excitonic and vibronic regimes, respectively. Section 7 contains the results of numerical simulations of the excitonic and vibronic spectra. In Sec. 8 we summarize the basic features concerning the manifestation of excitonic and vibronic spectra in 3D donor–acceptor crystals. Appendix A lists the classification of CTEs and FEs–CTEs coupling in the crystallographic point group $\bar{6}$.

2 CTEs in the Model of a 3D Hexagonal Crystal

The crystal's model consists of parallel donor layers and alternating acceptor layers. They form two hexagonal plane sublattices (x, y) displaced in a symmetric way (see Figure 1 and [1]). The open circles in Figure 1 represent the projections of acceptors on the plane of donors. The acceptor planes are situated at a distance $c/2$ relatively to the donor planes. The point group of this structure is $\bar{6}$ [1].

Let us consider the CTEs formed by a positive ion on the donor molecule (see Figure 2). The closest acceptor molecules create two symmetric triangles – one situated on the acceptor plane above the donor plane and the other – below it. In this way, six CTEs can ce created near the positive ion (nm). Due to the symme-

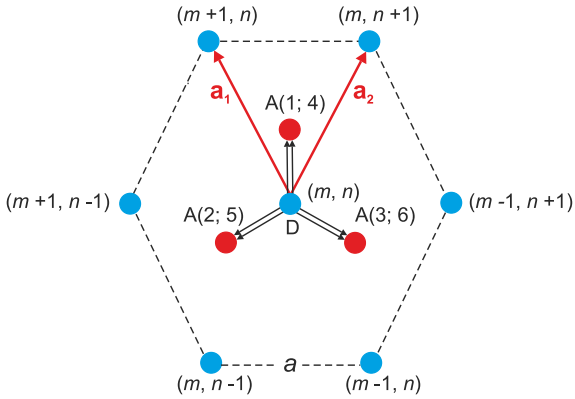

Figure 1. (Color online) Hexagonal sublattice plane of the centers of donor molecules (black). $(\vec{a}_1, \vec{a}_2)$ are 2D coordinate vectors, and a is the lattice constant. The acceptor A (open circles) planes are situated above $(1, 2, 3)$ and below $(4, 5, 6)$ that plane. The hexagonal acceptor sublattice is displaced in a symmetric way relatively to the nodes (nm) of donors' plane [1].

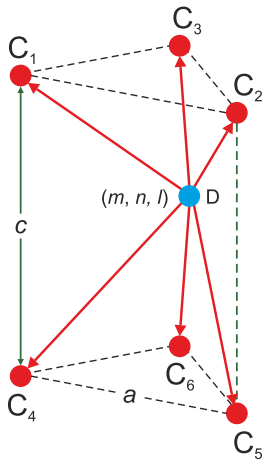

Figure 2. (Color online) Schematic view on the mutual positions of six CTEs (C_1,. . . ,C_6). Here, c is the length of the lattice unit vector parallel to the hexagonal axis z.

try operations, all CTEs correspond to identical quasiparticles. The CTEs transfer integrals describe the transfers of the holes on the neighbor donor molecules in the donor plane and the transfer of the CTEs's electron on the neighbor acceptors in their planes. Due to the third crystal's dimension the transfers of the holes between the two neighbor donor planes may be effective and the corresponding transformations of the CTEs must be taken into account (as well as the corresponding transfers of electrons between two neighbor acceptor planes).

First, we find the symmetry allowed combinations of CTEs in the point group $\bar{6}$. Consequently to the inversion center, the following two groups of CTEs states appear:

$$\Psi_{\mathrm{s,a}} = \left[a_1\left(C_1^+ \pm C_4^+\right) + a_2\left(C_2^+ \pm C_5^+\right) + a_3\left(C_3^+ \pm C_6^+\right)\right]|0\rangle, \quad (1)$$

where $C_{i,nml}^+ (i = 1\text{–}6)$ denote the operators of the corresponding CTEs with the hole on the donor (nml) (we do not write these subscripts in formula (1) and in the next expressions/equations). The coefficients a_i must be found by using the symmetry of six-fold axis [3]. It is easy to find out the relations:

$$a_1 = 1/\sqrt{6}, \qquad a_2 = a_1 \exp(\mathrm{i}\beta), \qquad a_3 = a_1 \exp(2\mathrm{i}\beta), \quad (2)$$

in which βs are the roots of the equation

$$\exp(3\mathrm{i}\beta) = 1; \qquad \beta = 2\pi/3, 4\pi/3, \text{ and } 2\pi. \quad (3)$$

Six linear combinations of CTEs states appear in the point group $\bar{6}$, notably

(A) Symmetric states

a) the states

$$\Psi_{1,2} = \frac{1}{\sqrt{6}}\Big[(C_1^+ + C_4^+) - \frac{1}{2}(C_2^+ + C_5^+ + C_3^+ + C_6^+) \pm \mathrm{i}\frac{\sqrt{3}}{2}(C_2^+ + C_5^+ - C_3^+ - C_6^+)\Big]|0\rangle, \quad (4)$$

in which the sign $+\mathrm{i}$ corresponds to $\beta = 2\pi/3$ and the sign $-\mathrm{i}$ to $\beta = 4\pi/3$. These combinations describe dipole active excitonic states with transition dipole moments

$$h(\hat{x} + \mathrm{i}\hat{y}), \qquad h(\hat{x} - \mathrm{i}\hat{y}), \quad (5)$$

where $\hat{x}$ and $\hat{y}$ are the unit vectors in the donor planes, while

b) the combination

$$\Psi_3 = \frac{1}{\sqrt{6}}\left[C_1^+ + C_2^+ + C_3^+ + C_4^+ + C_5^+ + C_6^+\right]|0\rangle \quad (6)$$

corresponds to $\beta = 2\pi$ and being totally symmetric possesses a vanishing transition electric dipole moment. It has a transition magnetic dipole moment R_z directed along the six-fold symmetry axis z [8].

(B) Antisymmetric states

a) the combinations

$$\Psi_{4,5} = \frac{1}{\sqrt{6}}\Big[(C_1^+ - C_4^+) - \frac{1}{2}(C_2^+ - C_5^+ + C_3^+ - C_6^+) \pm \mathrm{i}\frac{\sqrt{3}}{2}(C_2^+ - C_5^+ - C_3^+ + C_6^+)\Big]|0\rangle, \quad (7)$$

possess magnetic dipole transition moments $R(\hat{x} \pm \mathrm{i}\hat{y})$ [8];

b) CTEs combination

$$\Psi_6 = \frac{1}{\sqrt{6}} \left[C_1^+ - C_4^+ + C_2^+ - C_5^+ + C_3^+ - C_6^+ \right] |0\rangle \tag{8}$$

exhibits the following electric dipole transition moments along the z axis:

$$\hat{P}_{\mathrm{c},z} = p \left[C_1 - C_4 + C_2 - C_5 + C_3 - C_6 + \text{h.c.} \right]. \tag{9}$$

The CTEs part of the Hamiltonian includes the transfers of electrons and holes between the neighbor nods inside their planes (J_e and J_h are the corresponding transfer integrals), as well as the transfers at distance c between the neighbor planes of donors (acceptors) with the transfer interlayer integrals J_2 (for electrons) and J_3 (for holes). It reads

$$\begin{aligned}\hat{H}_{\mathrm{CTEs}} = \sum_{nml,\, i=1\text{–}6} \Big\{ & E_\mathrm{c} C_{i,nml}^+ C_{i,nml} \\ & + J_2 \left[C_{1,nml}^+ C_{4,nml} + C_{2,nml}^+ C_{5,nml} + C_{3,nml}^+ C_{6,nml} + \text{h.c.} \right] \\ & + J_3 \left[C_{1,nml-1}^+ C_{4,nml} + C_{2,nml-1}^+ C_{5,nml} \right. \\ & \left. + C_{3,nml-1}^+ C_{6,nml} + \text{h.c.} \right] + \hat{H}_{\mathrm{e,h}} \Big\}, \end{aligned} \tag{10}$$

in which E_c is the excitation energy of CTEs and $\hat{H}_{\mathrm{e,h}}$ is the 3D modification of the Hamiltonian in Ref. [3]. By using Fourier transforms of CTEs operators in the momentum space $\vec{k} = (k_1, k_2, k_3)$ one obtains

$$\begin{aligned}\hat{H}_{\mathrm{CTEs}} = \sum_{k,\, i=1\text{–}6} \Big\{ & E_\mathrm{c} C_{ik}^+ C_{ik} + \left[(J_2 + J_3 \exp(\mathrm{i}k_3 c)) \right. \\ & \left. \times \left(C_{1k}^+ C_{4k} + C_{2k}^+ C_{5k} + C_{3k}^+ C_{6k} \right) + \text{h.c.} \right] + \hat{H}_{\mathrm{e,h}} \Big\}, \end{aligned} \tag{11}$$

$$\begin{aligned}\hat{H}_{\mathrm{e,h}} = {} & J_\mathrm{e} \sum_k \left[C_{2k}^+ C_{1k} + C_{3k}^+ C_{2k} + C_{1k}^+ C_{3k} + C_{5k}^+ C_{4k} + C_{6k}^+ C_{5k} \right. \\ & \left. + C_{4k}^+ C_{6k} + \text{h.c.} \right] + J_\mathrm{h} \sum_k \left[C_{2k}^+ C_{1k} \exp(-\mathrm{i}k_1\gamma) \right. \\ & + C_{3k}^+ C_{2k} \exp(\mathrm{i}(k_1 - k_2)\gamma) + C_{1k}^+ C_{3k} \exp(\mathrm{i}k_2\gamma) \\ & + C_{5k}^+ C_{4k} \exp(-\mathrm{i}k_1\gamma) + C_{6k}^+ C_{5k} \exp(\mathrm{i}(k_1 - k_2)\gamma) \\ & \left. + C_{4k}^+ C_{6k} \exp(\mathrm{i}k_2\gamma) + \text{h.c.} \right], \end{aligned} \tag{12}$$

where $\gamma = a\sqrt{3}/2$.

3 Frankel Excitons–CTEs Coupling

Frenkel excitons in our model stem from the electronic excitation of a neutral donor molecule (see Sec. 1). In this section, we treat their coupling with the dipole active CTEs states (4) and (8). For completeness, the FEs–CTEs coupling terms of states (5) and (7) can be read in the Appendix.

Frenkel excitons with transition electric dipole moment along the symmetry axis z couple with CTEs of type (8). Then FE part of the Hamiltonian in the approximation of the nearest neighbors has the form:

$$\hat{H}_{\mathrm{F},z} = \sum_{k} \left[E_{\mathrm{F}} + 2W\mu(k_1,k_2) + 2W_1\cos(k_3 c)\right] B^{+}_{z,\mathbf{k}} B_{z,\mathbf{k}}, \tag{13}$$

in which E_{F} is the excitation energy of FE, $B_{z,\mathbf{k}}$ is its operator of annihilation and

$$W = \frac{p^2_{\mathrm{F},z}}{4\pi\varepsilon_0 a^3}, \qquad W_1 = -\frac{2p^2_{\mathrm{F},z}}{4\pi\varepsilon_0 c^3}, \tag{14}$$

$$\mu(k_1,k_2) = \cos(k_1\gamma) + \cos(k_2\gamma) + \cos\left[(k_1-k_2)\gamma\right], \tag{15}$$

where $p_{\mathrm{F},z}$ is the electric dipole transition moment of the FE state, and $\varepsilon_0 = 8.8542\times10^{-12}\ \mathrm{F\,m^{-1}}$ is the permittivity of free space.

Due to the axial symmetry, the coupling terms are relatively simple [2, 3]:

$$\hat{H}^{z}_{\mathrm{FE-CTEs}} = \varepsilon \sum_{k} \{[C^{+}_{1k} - C^{+}_{4k} + C^{+}_{2k} - C^{+}_{5k} + C^{+}_{3k} - C^{+}_{6k}]B_{z,k} + \mathrm{h.c.}\} \tag{16}$$

and the transition electric dipole moment of the coupled FE–CTEs states is the sum of operator (9) and the Frenkel exciton part, namely

$$\hat{P}^{z} = \{p\left[C_{1,k=0} - C_{4,k=0} + C_{2,k=0} - C_{5,k=0} + C_{3,k=0} - C_{6,k=0}\right] + p_{\mathrm{F},z}B_{z,k=0} + \mathrm{h.c.}\}. \tag{17}$$

Frenkel excitons with transition dipole moment $p_{\mathrm{F},xy}$ parallel to the donor layer are two-fold degenerate. Let x axis be directed along the transition dipole moment of the CTE($i=1$) parallel to the layer and the y axis is perpendicular to $\hat{x}$ and $\hat{z}$. Then the operator of the transition dipole moment reads [3]

$$\begin{aligned}\hat{P}^{xy} &= q\left[B_{x,k=0}\hat{x} + B_{y,k=0}\hat{y} + \mathrm{h.c.}\right] \\ &+ h\left\{\left[C_{1,k=0} + C_{4,k=0} - \frac{1}{2}\left(C_{2,k=0} + C_{5,k=0} + C_{3,k=0} + C_{6,k=0}\right)\right]\hat{x} \right. \\ &\left. + \frac{\sqrt{3}}{2}\left[C_{2,k=0} + C_{5,k=0} - C_{3,k=0} - C_{6,k=0}\right]\hat{y} + \mathrm{h.c.}\right\},\end{aligned} \tag{18}$$

where $B_{x,k}$ and $B_{y,k}$ represent the operators of annihilations of FEs with transition dipole moments along the x and y axes, respectively. The FE part of the (x, y) Hamiltonian is equal to

$$\hat{H}_{\mathrm{F},xy} = \sum_k \left[\left(E_{\mathrm{F},1} + W_{x,k} \right) B^+_{x,k} B_{x,k} + \left(E_{\mathrm{F},1} + W_{y,k} \right) B^+_{y,k} B_{y,k} \right], \quad (19)$$

where

$$W_{x,k} = 2V_1 \left\{ -\frac{5}{4} \left[\cos(k_1\gamma) + \cos(k_2\gamma) \right] + \cos[(k_1 - k_2)\gamma] \right\} + 2V_3 \cos(k_3 c), \quad (20a)$$

$$W_{y,k} = 2V_1 \left\{ \frac{1}{4} \left[\cos(k_1\gamma) + \cos(k_2\gamma) \right] - 2\cos[(k_1 - k_2)\gamma] \right\} + 2V_3 \cos(k_3 c), \quad (20b)$$

$$V_1 = q^2 / \left(4\pi\varepsilon_0 a^3 \right), \qquad V_3 = q^2 / \left(4\pi\varepsilon_0 c^3 \right). \quad (20c)$$

By using the results from Ref. [3], we find the following FE–CTEs coupling term:

$$\hat{H}^{x,y}_{\mathrm{FE–CTEs}} = \varepsilon_1 \sum_k \left\{ \left[C^+_{1k} + C^+_{4k} - \frac{1}{2} \left(C^+_{2k} + C^+_{5k} + C^+_{3k} + C^+_{6k} \right) \right] B_{x,k} + \frac{\sqrt{3}}{2} \left[C^+_{2k} + C^+_{5k} - C^+_{3k} - C^+_{6k} \right] B_{y,k} + \mathrm{h.c.} \right\}. \quad (21)$$

4 Exciton–Phonon Coupling

As it is in the previous papers [2, 3], one mode of the intramolecular vibrations of a donor or acceptor molecule is supposed to be coupled linearly with FEs and CTEs. Let a_{nml} be the annihilation operators of one quantum of intramolecular vibration on a donor or acceptor. Then the phonon and the exciton–phonon part of the Hamiltonian is as follows:

(a) Vibration on donors

$$\hat{H}_{\mathrm{exc–phon}} = \hbar\omega_0 \sum_{nml} a^+_{nml} a_{nml} + \xi_{\mathrm{F}} \hbar\omega_0 \sum_{nm} B^+_{nml} B_{nml} \left(a^+_{nml} + a_{nml} \right) + \xi\hbar\omega_0 \sum_{nml,\, i=1\text{–}6} C^+_{i,nml} C_{i,nml} \left(a^+_{nml} + a_{nml} \right), \quad (22)$$

where ω_0 is the vibrational frequency, ξ_{F} and ξ are the dimensionless parameters of FE–phonon and CTEs–phonon coupling parts, B_{nml} are the operators of

annihilation of FEs in the coordinate representation. The linear coupling terms can be eliminated by using the canonical transformation

$$\hat{H} = \exp(Q) H \exp(-Q), \tag{23}$$

in which

$$Q = \sum_{nml,\, i=1\text{–}6} \left[\xi_{\mathrm{F}} B^{+}_{nml} B_{nml} + \xi C^{+}_{i,nml} C_{i,nml} \right] \left(a^{+}_{nml} - a_{nml} \right), \tag{24}$$

and $\hat{H}$ is the sum of operators (10), (13), and (22), or (10), (19), and (22). Instead of operators B_{nml} and $C_{i,nml}$ the following transformed operators appear in the Hamiltonian, as well as in operators (17) and (18):

$$\begin{aligned} V_{nml} &= \exp(Q) B_{nml} \exp(-Q) \quad \text{and} \\ U_{i,nml} &= \exp(Q) C_{i,nml} \exp(-Q). \end{aligned} \tag{25}$$

(b) Vibration on acceptors

Analogous formulae with $\xi_{\mathrm{F}} = 0$ describe exciton–phonon coupling in the case of intramolecular vibrations on acceptors.

5 Linear optical susceptibility in excitonic regime

The following formulae have been used in calculating the linear optical susceptibility χ_{ij} [4,5]:

$$\chi_{ij} = \lim_{\varepsilon \to +0} \left\{ -\frac{1}{2\hbar V} \left[\Phi_{ij}(\omega + \mathrm{i}\varepsilon) + \Phi_{ij}(-\omega + \mathrm{i}\varepsilon) \right] \right\}, \tag{26}$$

where V is the volume of the crystal, and

$$\Phi_{ij}(t) = -\mathrm{i}\theta(t) \langle 0 | \hat{P}_i(t) \hat{P}_j(0) + \hat{P}_j(t) \hat{P}_i(0) | 0 \rangle, \tag{27}$$

with the operator $\hat{P}$ given by formulae (17) and (18). The Green functions (27) have been calculated as an average over only the ground state $|0\rangle$ taking into account the large values of $E_{\mathrm{F}}, E_{\mathrm{c}}, \hbar\omega_0 \gg k_{\mathrm{B}} T$. The calculations have been performed using the vibronic approach [9] which is valid in the case of small values of the transfer and coupling parameters compared with $\hbar\omega_0$. In the following we reproduce the final formulae of χ_{ij} obtained by means of the approach used in the previous papers [2, 3] for the excitonic regime and and for the one-phonon vibronic spectra in Sec. 6.

The χ_{zz} component (for the light polarized along the symmetry axis) is (see Eq. (17))

$$\chi_{zz} = -\frac{1}{v \left(\alpha_{11} \alpha_{22} - 6\alpha_{12}^2 \right)} \left[p_{\mathrm{F},z}^2 \alpha_{22} + 12 \alpha_{12} p_{\mathrm{F},z} p + 6 p^2 \alpha_{11} \right], \tag{28}$$

where

$$\begin{aligned}\alpha_{11} &= \hbar\,(\omega - \Omega_{0\mathrm{F}}) - (E_{\mathrm{F}} + 6W + 2W_1)\,,\\ \alpha_{12} &= \varepsilon,\\ \alpha_{22} &= \hbar\,(\omega - \Omega_{0\mathrm{c}}) - (E_{\mathrm{c}} + 2J_{\mathrm{e}} + 2J_{\mathrm{h}} - J_2 - J_3)\,.\end{aligned} \tag{29}$$

Functions $\Omega_{0\mathrm{F}}$ and $\Omega_{0\mathrm{c}}$ are expressed via the following continuous fractions:

$$\Omega_{0\mathrm{F}} = \cfrac{\omega_{\mathrm{F}}^2}{\omega - E_{\mathrm{F}}/\hbar - \omega_0 - \cfrac{2\omega_{\mathrm{F}}^2}{\omega - E_{\mathrm{F}}/\hbar - 2\omega_0 - \cfrac{3\omega_{\mathrm{F}}^2}{\cdots}}}, \tag{30a}$$

$$\Omega_{0\mathrm{c}} = \cfrac{\omega_a^2}{\omega - E_{\mathrm{c}}/\hbar - \omega_0 - \cfrac{2\omega_a^2}{\omega - E_{\mathrm{c}}/\hbar - 2\omega_0 - \cfrac{3\omega_a^2}{\cdots}}}, \tag{30b}$$

where $\omega_{\mathrm{F}} = \xi_{\mathrm{F}}\omega_0$ and $\omega_a = \xi\omega_0$. The $\chi_{xx} = \chi_{yy}$ components for the light polarized perpendicular to the symmetry axis are given by the following expression

$$\chi_{xx} = \chi_{yy} = -\frac{1}{v\,(\alpha_{11}\alpha_{22} - 3\alpha_{12}^2)}\left[q^2\alpha_{22}^2 + 6\alpha_{12}hq + 3\alpha_{11}h^2\right], \tag{31}$$

in which v is the volume occupied by one D–A pair, components h and q have been defined by Eq. (18), and here

$$\begin{aligned}\alpha_{11} &= \hbar\,(\omega - \Omega_{0\mathrm{F}}) - (E_{\mathrm{F}} + 2V_3 - 3V_1)\,,\\ \alpha_{12} &= \varepsilon_1,\\ \alpha_{22} &= \hbar\,(\omega - \Omega_{0\mathrm{c}}) - (E_{\mathrm{c}} - J_{\mathrm{e}} - J_{\mathrm{h}} + J_2 + J_3)\,.\end{aligned} \tag{32}$$

6 Linear Optical Susceptibility in Vibronic Regime

The calculations of χ_{ij} in one-phonon vibronic regime follow the methods of Ref. [2, 3]. The χ_{zz} component is given by formula (28) and the $\chi_{xx} = \chi_{yy}$ components by formula (31). Functions α_{11}, α_{22}, and α_{12} in the case of more stronger interlayer transfers, described by the parameters J_2 and J_3, and very small inlayer transfers of CTEs (J_{e}, J_{h}, and the operator $\hat{H}_{\mathrm{e,h}}$ being considered negligible) have been calculated in the similar way as we did in the 2D geometry (see Ref. [3]). The opposite case of negligible interlayer transfer (very small values of J_2 and J_3) has been treated in the 2D case in Ref. [3]. In the present paper, we calculate the linear absorption for a 3D crystal and compare with the results of the 2D crystal.

7 Simulations of the linear absorption spectra

The experimental data of the linear absorption spectra in a two-component crystal of the crystallographic point group $\bar{6}$ are absent and we use several sets of typical values of the excitonic and vibrational parameters. In the figure's captions we give the corresponding sets for each calculated curve.

Figures 3 and 4 are based on formulae (28) and (31). They illustrate the general structure of the electronic and vibronic spectra. The lineshape of all spectral lines is Lorentzian with half-width which is given by the imaginary part

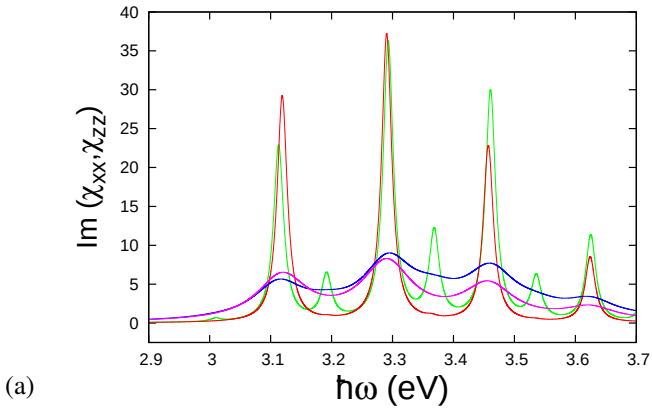

Figure 3. (Color online) Linear absorption spectra in excitonic regime: $E_{\mathrm{F}} = 3.30$ eV, $E_{\mathrm{c}} = 3.20$ eV, $\hbar\omega_0 = 0.17$ eV, $\xi_{\mathrm{F}} = 1.05$, $\xi = 0.72$, $J_{\mathrm{e}} = -J_{\mathrm{h}} = 0.004$ eV, $J_2 = 0.004$ eV, $J_3 = -0.003$ eV, $W = 0.0035$ eV, $W_1 = -0.021$ eV, $V_1 = -0.0044$ eV, $V_3 = 0.01$ eV, $\varepsilon = 0.005$ eV (for χ_{zz}), $\varepsilon_1 = 0.05$ eV (for χ_{xx}), $p/p_{\mathrm{F},z} = 0.03$ (for χ_{zz}), and $h/q = 0.3$ (for χ_{xx}): (a) $\hbar\delta = 0.01$ eV (red curve χ_{zz}, green curve χ_{xx}) and $\hbar\delta = 0.05$ eV (purple curve χ_{zz}, blue curve χ_{xx}); (b) $\hbar\delta = 0.001$ eV (red curve χ_{zz}, green curve χ_{xx}).

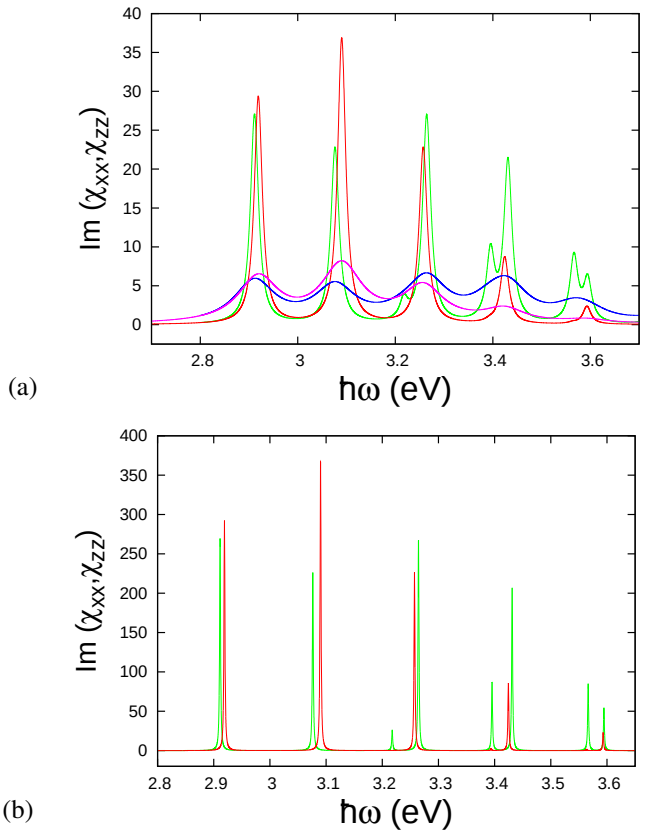

Figure 4. (Color online) Linear absorption spectra in excitonic regime: $E_{\rm F} = 3.10$ eV, $E_{\rm c} = 3.40$ eV. For the other data and curves' colors see Figure 3.

of the frequency $\omega + {\rm i}\delta$ (δ expresses the excitonic damping). In Figures 3(a) and 4(a) we we take the values $\hbar\delta = 0.01$ eV (red curve ξ_{zz}, and green curve ξ_{xx}) and $\hbar\delta = 0.05$ eV (purple curve ξ_{zz}, and blue one ξ_{xx}). Thes values describe the spectra of several DA crystals. In Figures 3(b), 4(b), and 5–9 the value of excitonic damping that we have used was $\hbar\delta = 0.001$ eV. The weak damping manifests the fine structure of the spectra and can be used for their interpretation. The spectra in Figure 3 consist of excitonic part (below 3.15 eV), one-phonon vibronic spectra (the region of 3.18–3.3 eV), two-phonon vibronic spectra (3.36–3.45 eV), three-phonon vibronic spectra (3.53–3.65 eV), etc. The manifestation of CTEs near 3.0 eV is very weak but its vibronic replicas near 3.20, 3.37, and 3.54 eV are influenced by the FEs–CTEs coupling which makes the spectral lines of CTEs and FEs (at 3.11, 3.29, 3.46 and 3.64 eV) of comparable intensity.

The CTEs manifest themselves in the $(x$–$y)$-plane and thus the red and purple curves are influenced very weakly by the FE–CTEs coupling and represent the absorbtion spectra of Frenkel excitons only. The FE–CTEs splitting demonstrates itself at intermediate dampings (green curve) whereas the blue curve (at $\hbar\delta = 0.05$ eV) does not exhibit the CTEs maxima at 3.20, 3.37, and 3.54 eV.

The distance between E_{F} and E_{c} in Figure 4 is supposed to be larger than $\hbar\omega_0$ ($E_{\mathrm{c}} - E_{\mathrm{F}} = 0.30$ eV $\approx 2\hbar\omega_0$) and one obtains two series of excitonic spectra and their vibronic wings. The FE lines are positioned near 2.9 eV – their vibronic states lie near 3.08, 3.27, 3.43, and 3.60 eV. The CTEs lines are positioned near 3.21 eV (very weak) and their vibronic wings appear near 3.39 and 3.57 eV. The splitting of both polarizations along symmetric axis ($\mathrm{Im}\chi_{zz}$ in red) and perpendicular to it ($\mathrm{Im}\chi_{xx}$ in green) is well exposed in the pure FE lines and one=phonon FE lines (below 3.1 eV). As it is in Figure 3, the strong damping $\hbar\delta = 0.05$ eV cancels the effects of FE–CTEs splitting.

Figures 5–9 have been calculated using vibronic formulas. Strictly speaking, our calculations describe one-phonon vibronic spectra but they can be used for simulations of two-phonon spectra, too. In Figure 5, the one-phonon vibronic spectra lie in the region of 3.22–3.35 eV whereas the absorption lines above 3.41 eV correspond to two-phonon vibronics. We note the weak CTEs vibronic lines near 3.23 and 3.41 eV along with strong doublets of FEs satellites near 3.33 and 3.49 eV. The doublet of one-phonon and two-phonon vibronic spectra can be interpreted as a manifestation of the six-fold symmetry (compare with the 2D case in Ref. [3]).

Figures 6 and 7 correlate to Figure 4 ($E_{\mathrm{F}} = 3.10$ eV, $E_{\mathrm{c}} = 3.40$ eV) taking into account the intermolecular transfers of FEs, described by the parameters

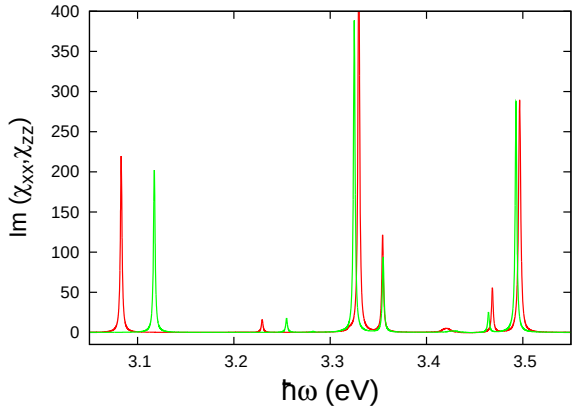

Figure 5. (Color online) Linear absorption spectra in vibronic regime using the parameters of Figure 3 and $\varepsilon = 0.05$ eV. Red curve: $\mathrm{Im}\chi_{zz}$, green curve: $\mathrm{Im}\chi_{xx}$.

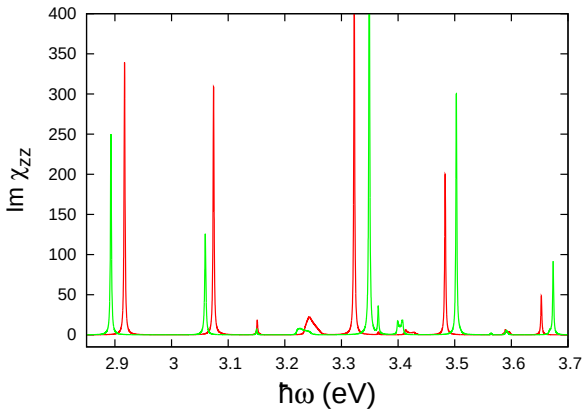

Figure 6. (Color online) Linear absorption spectra of the z polarization ($\mathrm{Im}\chi_{zz}$) in vibronic regime using the parameters of Figure 4 with $W = 0.0035$ eV and $W_1 = -0.021$ eV. Red curve: $\varepsilon = 0.01$ eV, green curve: $\varepsilon = 0.05$ eV.

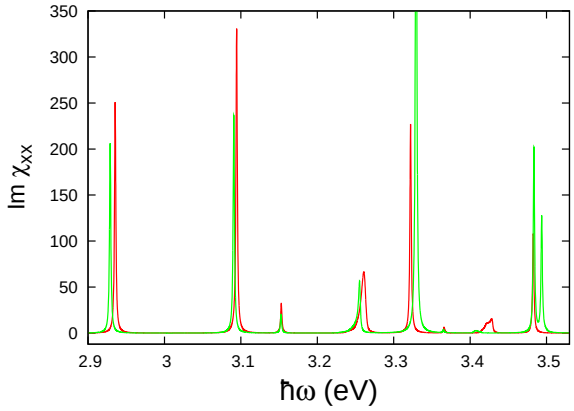

Figure 7. (Color online) Linear absorption spectra of the (xy) polarization ($\mathrm{Im}\chi_{xx}$). For the parameters see Figure 4 with $V_1 = -0.0044$ eV and $V_3 = 0.01$ eV. Red curve: $\varepsilon = 0.01$ eV, green curve: $\varepsilon = 0.05$ eV.

W, W_1, V_1, V_3 (see Sec. 3). Due to the FEs–CTEs coupling and the transfers of FEs, the absorption lines of CTEs near 3.25 and 3.42 eV are widen. Their lineshape is not Lorentzian and it depends upon the dispersion in the excitonic bands of FEs.

Figures 8 and 9 have been calculated in the case of negligible interlayer transfer of CTEs ($J_2 = J_3 = 0$) and in the case of essential transfer of CTEs in the donor and acceptor planes ($J_\mathrm{e}, J_\mathrm{h} \neq 0$). In the same figures we compare the linear ab-

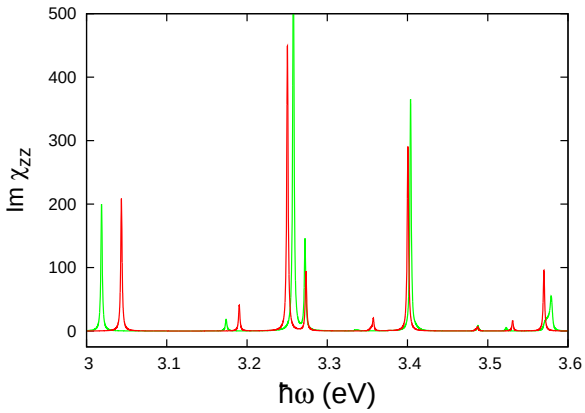

Figure 8. (Color online) Linear absorption spectra ($\mathrm{Im}\chi_{zz}$) in the case of strong in-plane transfer of CTEs ($J_2 = J_3 = 0$, $J_\mathrm{e} = 0.004$ eV, $J_\mathrm{h} = -0.003$ eV): $E_\mathrm{F} = 3.22$ eV, $E_\mathrm{c} = 3.30$ eV, $\hbar\omega_0 = 0.17$ eV, $\varepsilon = 0.031$ eV, $\xi_\mathrm{F} = 1.05$, $\xi = 0.72$, $W = 0.0035$ eV, and $W_1 = -0.021$ eV. Red curve: the 3D case, green curve: the 2D case of a hexagonal lattice of donors and acceptors (Ref. [3]).

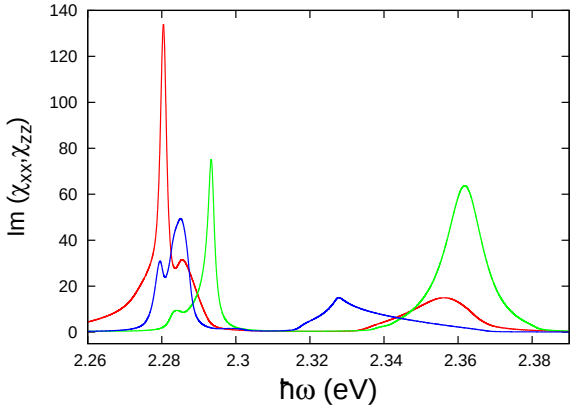

Figure 9. (Color online) One-phonon vibronic spectra in the case of weak exciton–phonon coupling ($\xi_\mathrm{F} = 0.6$, $\xi = 0.4$): $E_\mathrm{F} = 2.23$ eV, $E_\mathrm{c} = 2.15$ eV, $\hbar\omega_0 = 0.17$ eV, $\varepsilon = -0.02$ eV, $J_\mathrm{e} = -J_\mathrm{h} = 0.004$ eV, $J_2 = J_3 = 0$, $W = 0.01$ eV, and $W_1 = -0.02$ eV. Red curve: the 3D case (in the present paper, $\mathrm{Im}\chi_{zz}$), green curve: the 2D case ($\mathrm{Im}\chi_{zz}$), blue curve: the 2D case ($\mathrm{Im}\chi_{xx}$). The green and blue curves have been calculated in Ref. [3].

sorption in the 3D case under consideration and in the case of a 2D hexagonal lattice of donors and acceptors (see Ref. [3]). The comparison of the red curve (3D case) and the green curve (2D case) in Figure 8 exhibits some amplification

of the CTEs lines near 3.19 and 3.36 eV but they seem to be weak and difficult to be observed. The situation in Figure 9 (weak exciton–phonon coupling) is rather different. One-phonon vibronic spectra consist of two bands of unbound exciton–phonon states: the lower (2.27–2.30 eV) and the upper (2.32–2.38 eV) bands correspond to an unbound propagation of excitons and phonons and describe many-particle exciton–phonon states. The lineshape of the red curve (3D case) depends on the density of states in excitonic bands (13) while the other two curves (2D case) depend on the peculiarities of the excitonic bands in the model of a two-dimensional donor–acceptor lattice (Ref. [3]).

8 Conclusion

The present paper contains the theoretical analysis of the excitonic spectra in a two-component crystal of the crystallographic point group $\bar{6}$. We have used as a model an actually synthesized crystal [1] with two types of organic molecules positioned in parallel layers, each one consisting of one-component molecules with hexagonal ordering. This model represents the 3D spatial model of the graphene-like 2D lattice of donors and acceptors [3]. The model includes both Frenkel excitons of excited neutral molecules and charge transfer excitons of ionized donor and acceptor molecules alongside their coupling and the coupling of both types of excitons with one mode of intramolecular vibration. In the paper, the symmetry governs combinations of CTEs and FEs and consequently an anisotropy of the FEs–CTEs coupling has been established. We considered the case in which Frenkel excitons and the mode of intramolecular vibrations belong to the same entity (donor or acceptor). The case of different origin of FEs and the vibrational mode is very similar but it requires a special treatment.

The natural anisotropy of the model in the direction along the six-fold axis and in directions perpendicular to it causes a splitting in the linear absorption spectra along with a FEs–CTEs splitting. Our simulations demonstrate a more significant splitting in pure excitonic spectra and eventually in one-phonon vibronic spectra, whereas in the higher vibronic satellites the anisotropic splitting is relatively weaker. That splitting can be, however, suppressed by the strong excitonic damping (see Figures 3 and 4). In the case of weak and intermediate damping the observation of details in absorption spectra could be realistic (see the analysis of the excitonic and vibronic spectra of the anthracene-PMDA crystal [7]). The numerical simulations of the linear absorption spectra exhibit both types of exciton–phonon states, notably one -particle (bound) states with Lorentzian lineshape and many-particle (unbound) states with wide and complicated lineshapes – compare Figures 5 and 9. Parameters that produce different vibronic spectra are the coefficients of exciton–phonon coupling ξ and ξ_{F}. In the case of $\xi_{\mathrm{F}}, \xi > 1$ the one-particle states manifest themselves and if $\xi_{\mathrm{F}}, \xi < 1$ the unbound exciton–phonon states will produce wide vibronic lineshapes.

Our analysis exposes the classification, coupling and manifestation of excitations in 3D molecular structures of high symmetry.

Acknowledgments

The authors would like to thank Professor Stoyan Roussev for providing information about the optical properties of the crystal's two components and Dr. Snezhana Yordanova for drawing two figures.

Appendix

FE–CTEs coupling of excitations with zero transition electric dipole moment

(i) Totally symmetric excitations (representation A′ in point group $\bar{6}$)

Frenkel excitons:

$$\hat{H}_{\mathrm{FE}}^{(\mathrm{A}')} = E_{\mathrm{F}z} \sum_{k,\, k=1\text{–}6} A_k^+ A_k,$$

Charge transfer excitons:

$$\Psi_3 = \frac{1}{\sqrt{6}} \left[C_1^+ + C_2^+ + C_3^+ + C_4^+ + C_5^+ + C_6^+ \right] |0\rangle,$$

FE–CTEs coupling:

$$\hat{H}_{\mathrm{FE–CTEs}}^{(\mathrm{A}')} = \sum_{k,\, k=1\text{–}6} \left(C_{i,k}^+ A_k + \mathrm{h.c.} \right).$$

(ii) Excitations of representation E″

Frenkel excitons:

$$\hat{H}_{\mathrm{FE}}^{(\mathrm{E}'')} = E_{\mathrm{F}3} \sum_k \left(F_{x,k}^+ F_{x,k} + F_{y,k}^+ F_{y,k} \right),$$

Charge transfer excitons:

$$\Psi_{4,5} = \frac{1}{\sqrt{6}} \left[\left(C_1^+ - C_4^+ \right) - \frac{1}{2} \left(C_2^+ - C_5^+ + C_3^+ - C_6^+ \right) \right.$$
$$\left. \pm \mathrm{i} \frac{\sqrt{3}}{2} \left(C_2^+ - C_5^+ - C_3^+ + C_6^+ \right) \right] |0\rangle,$$

FE–CTEs coupling:

$$\hat{H}^{(\mathrm{E}'')}_{\mathrm{FE\text{–}CTEs}} = \varepsilon_3 \sum_k \left\{ \left[C^+_{1,k} - C^+_{4,k} - \frac{1}{2}\left(C^+_{2,k} - C^+_{5,k} + C^+_{3,k} - C^+_{6,k} \right) \right] F_{x,k} + \frac{\sqrt{3}}{2}\left[C^+_{2,k} - C^+_{5,k} - C^+_{3,k} + C^+_{6,k} \right] F_{y,k} + \text{h.c.} \right\}.$$

References

[1] V.R. Thalladi, K. Panneerselvam, C.J. Carrell, H.L. Carrell, and G.R. Desiraju (1995) *J. Chem. Soc., Chem. Commun.* **3** 341.

[2] I.J. Lalov, C. Warns, and P. Reineker (2008) *New J. Phys.* **10** 085006.

[3] I.J. Lalov and I. Zhelyazkov (2015) *Bulg. J. Phys.* **42** 172.

[4] A.S. Davydov (1971) *Theory of Molecular Excitons*, Plenum, New York.

[5] V.M. Agranovich (2009) *Excitations in Organic Solids*, Oxford University Press, New York.

[6] D. Haarer and M.R. Philpott (1983) in *Spectroscopy and Excitation Dynamics of Condensed Molecular Systems*, eds. V.M. Agranovich and R.M. Hochstrasser, North-Holland, Amsterdam, Chap. 2.

[7] A. Brillante and M.R. Philpott (1980) *J. Chem. Phys.* **72** 4019.

[8] R.L. Flurry, Jr. (1980) *Symmetry Groups Theory and Chemical Applications*, Prentice-Hall, Upper Saddle River, NJ 07458.

[9] I.J. Lalov and I. Zhelyazkov (2007) *Phys. Rev.* B **75** 245435.